発表者氏名	論文タイトル名	発表誌名	巻号	ページ	出版年
Y. Lee, K. Kataoka, et al.	Charge-conversion ternary polyplex with endosome disruption moiety: A technique for efficient and safe gene delivery.	Angew. Chem., Int. Ed.	47	5163-5166	2008
S. Takae, K. Kataoka, et al.	EG-detachable polyplex micelles based on disulfide-linked block catiomers as bioresponsive nonviral gene vectors.delivery.	J. Am. Chem. Soc.	130	6001-6009	2008

Protein Delivery

DOI: 10.1002/anie.200900064

Charge-Conversional Polyionic Complex Micelles—Efficient Nanocarriers for Protein Delivery into Cytoplasm**

*Yan Lee, Takehiko Ishii, Horacio Cabral, Hyun Jin Kim, Ji-Hun Seo, Nobuhiro Nishiyama, Hiroki Oshima, Kensuke Osada, and Kazunori Kataoka**

In the postgenomic era, the elucidation of protein function is one of the most important challenges in biological fields as the development of protein-based therapeutics has great potential in medicinal science. Enhancement and knockout of a specific protein expression are among the various methods that have been used for fundamental research into protein function. The direct delivery of proteins into cells is probably one of the simplest and most decisive ways to examine protein function, as no interference or artifacts occur during the transcription–translation pathway. Moreover, an efficient in vivo protein delivery is essential for therapeutic applications. Although various protein-based biopharmaceuticals have been developed, the instability of proteins in serum and the lack of a delivery method into cytoplasm has limited further success.[1] Many research groups have therefore concentrated on the development of protein delivery methods[2] such as hydrogels, liposomes, nanotubes, or inorganic carriers, but a highly efficient delivery method that offers serum stability and generality has not yet been developed.

We report herein a novel approach for protein delivery based on polyionic complex (PIC) micelles, which are well-defined core–shell supramolecular structures formed through electrostatic interactions when diblock copolymers with both a neutral and an ionic block mix with their counterions.[3] Because the shell of the neutral block protects the core from external deactivation pathways such as enzymatic attack or aggregation, the PIC micelle can act as a molecular container. PIC micelles have also been used as delivery carriers for drugs or biomacromolecules because of their high stability, reduced immune response, and elongated circulation time, which arise from their biocompatible surfaces and high molecular weights.[4] We have successfully developed PIC micelles, which contain a block copolymer with poly(ethylene glycol) (PEG) as a neutral block and a poly(amino acid) as an ionic block,[5] for DNA and RNA delivery. However, the protein-containing PIC micelles dissociated immediately at a physiological salt concentrations, which has limited their biological application.[6] Stabilized PIC micelles could be obtained by cross-linking with glutaraldehyde; it was difficult to apply these micelles in the human body because of the toxicity of glutaraldehyde and the irreversibility of the cross-linking.[7] The salt stability of the PIC micelles is closely related to the charge density of its components. For example, PIC micelles of DNA with high charge density (−308 Da per charge) were stable, but those with lysozyme (+1980 Da per charge) dissociated rapidly at the physiological salt concentration.

Therefore, in order to obtain a higher micelle stability, we attempted to increase the charge density of the protein by employing a reversible conjugation. Citraconic amide and *cis*-aconitic amide, derivatives of the maleic acid amide, are stable at the normal physiological pH value of 7.4, but degrade at the endosomal pH value of 5.5 to expose primary amines, with a charge conversion from negative to positive.[8] If a protein has a sufficient amount of lysine groups that can be modified to citraconic amides or *cis*-aconitic amides, the pI (isoelectric point) of the protein decreases significantly. Moreover, because the *cis*-aconitic amide exposes two carboxylate groups per reacted amine group, the anionic charge density could be reversibly increased (Scheme 1). We expected that the PIC micelles that contain the modified protein would have an increased salt stability because of the high charge density, and that they could release the original protein after charge conversion in the endosome.

We selected equine heart cytochrome c (CytC; M_w = 12384 Da), an essential protein in the electron transfer of the mitochondria, as a model protein. The CytC is a cationic protein with a charge density of +1391 Da per charge, which arises from the presence of three aspartate, nine glutamate, two arginine, and 19 lysine units. However, CytC could not form the PIC micelles with poly(ethylene glycol)–poly[(*N*-succinyl-2-aminoethyl(aspartamide)] (PEG–pAsp(EDA-Suc); **2**), an anionic block copolymer, in the presence of NaCl (150 mM). We modified CytC with citraconic anhydride and *cis*-aconitic anhydride to increase the charge density (the synthetic procedure for all block copolymers and the CytC modification method are described in detail in the Supporting Information). The resulting anionic proteins were Cyt–Cit (−501 Da per charge) and Cyt–Aco (−320 Da per charge).

[*] Dr. Y. Lee, Dr. H. Cabral, Dr. N. Nishiyama, Prof. Dr. K. Kataoka
Center for Disease Biology and Integrative Medicine
Graduate School of Medicine, The University of Tokyo
7-3-1 Hongo, Bunkyo-ku, Tokyo 113-0033 (Japan)
Fax: (+81) 3-5841-7139
E-mail: kataoka@bmw.t.u-tokyo.ac.jp
Dr. T. Ishii, Prof. Dr. K. Kataoka
Department of Bioengineering, The University of Tokyo
7-3-1 Hongo, Bunkyo-ku, Tokyo 113-8656 (Japan)
H. J. Kim, J. Seo, H. Oshima, Dr. K. Osada, Prof. Dr. K. Kataoka
Department of Materials Engineering, The University of Tokyo
7-3-1 Hongo, Bunkyo-ku, Tokyo 113-8656 (Japan)
Dr. N. Nishiyama, Prof. Dr. K. Kataoka
Center for Nanobio Integration, The University of Tokyo
7-3-1 Hongo, Bunkyo-ku, Tokyo 113-8656 (Japan)

[**] This work was supported by a Core Research for Evolutional Science and Technology (CREST) grant from the Japan Science and Technology Agency (JST).

Supporting information for this article is available on the WWW under http://dx.doi.org/10.1002/anie.200900064.

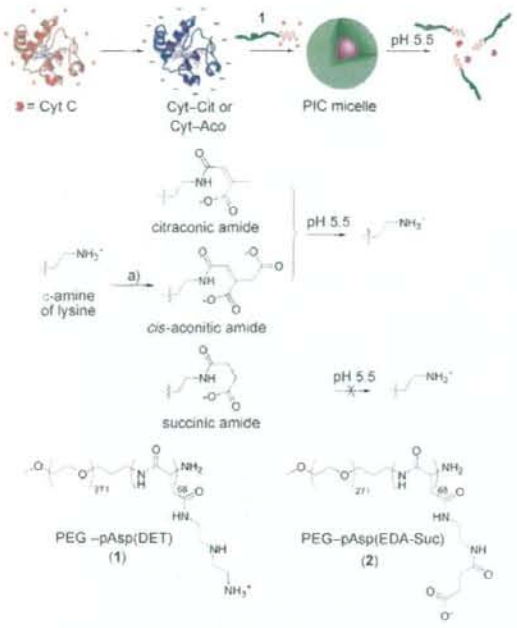

Scheme 1. Schematic representation showing the preparation of the charge-conversional PIC micelles containing CytC derivatives and PEG–pAsp(DET). a) Citraconic anhydride (or *cis*-aconitic anhydride/ succinic anhydride).

The formation of the PIC micelle containing the modified CytC and a block copolymer, PEG–poly[*N*-{*N'*-(2-aminoethyl)-2-aminoethyl}aspartamide] (PEG–pAsp(DET); **1**), was examined because PEG–pAsp(DET) has been reported to efficiently deliver DNA into cytoplasm and to have minimal toxicity.[9] The pH-sensitive endosome-destabilization activity of the pAsp(DET) block was shown to be the main reason for the high delivery efficiency.[10] Dynamic light scattering (DLS) measurements showed the PIC micelles to have a unimodal size distribution with diameters of about 50 nm and PDI values of about 0.05, even at physiological salt concentration (150 mM NaCl; Table 1). The spherical shape of the micelles was confirmed by using AFM (Figure 1). The spherical PIC micelles were formed at the N/C (amine/carboxylate) ratio of 2. Considering that one *N'*-(2-aminoethyl)-2-aminoethyl group has one positive charge at pH 7.4[11] because of the pKa difference between two amines, the PIC micelles could be formed at the charge ratio (+/−) of 1. Consequently, we succeeded in forming stable and stoichiometric PIC micelles under physiological salt conditions, by increasing the charge density of the protein without cross-linking.

Table 1: The formation of the PIC micelles between the block copolymer and CytC derivatives.

Protein	Charge density [Da per charge][a]	pI[a]	Diameter [nm][b]	PDI[b]
CytC[c]	+1391	9.57	n.d.	n.d.
Cyt–Cit[d]	−501	3.71	43.3	0.046
Cyt–Aco[d]	−320	3.47	50.1	0.055

[a] The calculation is described in the Supporting Information. [b] Determined by using DLS. [c] Compound **2** was used as the anionic block copolymer. [d] Compound **1** was used as the cationic block copolymer.

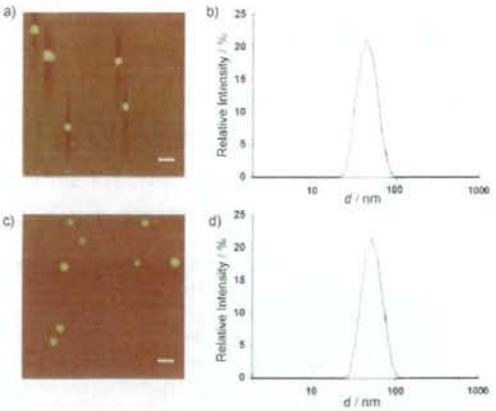

Figure 1. AFM images of the PIC micelles containing a) Cyt–Cit and c) Cyt–Aco. DLS distributions of the PIC micelles containing b) Cyt–Cit and d) Cyt–Aco (N/C ratio = 2). Scale bars: 200 nm.

The resulting citraconic amide and *cis*-aconitic amide in Cyt–Cit and Cyt–Aco showed rapid degradability at pH 5.5 (see Figure S1 in the Supporting Information). At pH 5.5, about 80% of the modified lysine reverted to the original lysine within 2 hours, whereas at pH 7.4, only 20–30% reverted, even after 24 hours. As the degradation took place concurrently with the charge conversion from negative to positive, the corresponding dissociation of the PIC micelles was expected to occur. The dissociation was analyzed by using the fluorescence quenching–dequenching method.[12] The fluorescence intensity of the Alexa Fluor 488 labeled CytC derivatives in the core of the PIC micelles was reduced significantly because of the probe–probe quenching effect (<20%). However, the protein release from the PIC micelles induced the recovery of the fluorescence intensity (Figure 2). Over 50% of Cyt–Cit was released from the PIC micelles within 4 hours at pH 5.5, whereas only 10% was released even after 8 hours at pH 7.4. Experiments with Cyt–Aco showed similar release profiles but with a slower rate, which is probably because Cyt–Aco has a higher charge density than Cyt–Cit. The bioactivity of the released CytC from the PIC micelles was also analyzed with a 2,2'-azino-bis(3-ethylbenzthiazoline-6-sulfonic acid) (ABTS) assay (see Figure S4 in the Supporting Information).[13] No difference was observed between the released CytC and the native CytC, which means that the modification–reversion cycle does not affect the activity of CytC. Because the only modification was the change of the amino acids from hydrophilic (+) to hydrophilic (−), extreme conformational denaturation that affected the protein activity was probably limited.

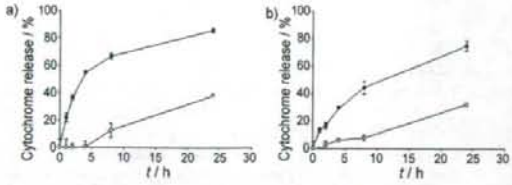

Figure 2. Release of the CytC derivatives from the PIC micelles containing a) Cyt–Cit and b) Cyt–Aco at 37 °C at pH 5.5 (●) and pH 7.4 (○). Each error bar represents the standard deviation of three experiments.

Finally, the delivery efficiency of the charge-conversional PIC micelles on a human hepatoma cell line (HuH-7) was examined. The intracellular distribution of the CytC derivatives labeled with Alexa Fluor 488 (green) was investigated by using confocal laser scanning microscopy (CLSM). The cell images after incubation for 24 h are shown in Figure 3. Because the late endosome and lysosome were stained by LysoTracker Red (red), the CytC in the endosome was detected as yellow. The yellow fluorescence turned to green after protein release from the endosome (see Figure S5 in the Supporting Information for the quantification of the green and red fluorescence colocalization). The native CytC and succinyl CytC (Cyt–Suc), the non-charge-conversional anionic derivative, were used as the controls. As shown in Figure 3a, almost no green fluorescence was detected when the cells were incubated with the native CytC. The lack of green fluorescence was expected, because it is difficult for hydrophilic proteins to penetrate through the plasma membrane. The cells incubated by the PIC micelles containing Cyt–Suc and the polymer **1** showed approximately yellow fluorescence (colocalization ratio (CR) = 0.803); Figure 3b), which means that significant cellular uptake but no endosomal escape occurred. Because the PIC micelles containing Cyt–Suc and **1** did not show any dissociation, even after 24 h at pH 5.5 (see Figure S3 in the Supporting Information), the low efficiency of the endosomal escape is quite reasonable when it is considered that direct contact between the cationic (pAsp(DET)) block and endosomal membrane is important for endosomal escape to occur.[14]

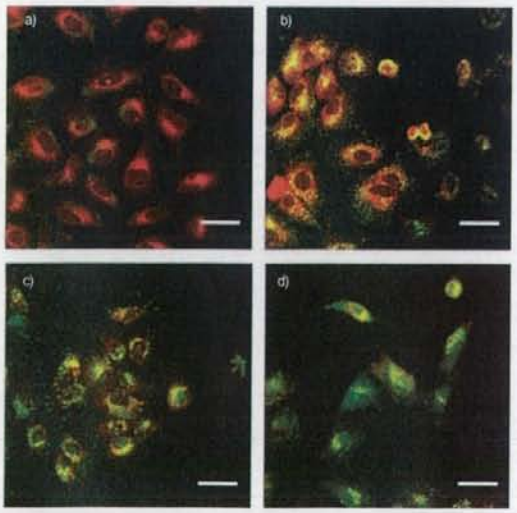

Figure 3. CLSM images of HuH-7 delivered by a) free native CytC, b) Cyt–Suc PIC, c) Cyt–Aco PIC, and d) Cyt–Cit PIC micelles after 24 h transfection. Each CytC derivative was labeled with Alexa Fluor 488 (green). The late endosome and lysosome were stained with LysoTracker Red (red). Scale bars: 50 μm.

In contrast, the charge-conversional PIC micelles containing Cyt–Aco or Cyt–Cit showed strong green fluorescence as well as yellow fluorescence (Figure 3c,d). It was assumed that the polymer **1** released from the PIC micelle could come into direct contact with the endosomal membrane to induce the efficient escape of the CytC. When the two charge-conversional PIC micelles are compared, micelles containing Cyt–Cit (CR = 0.498) showed more efficient endosomal release and resulting cytosolic distribution than Cyt–Aco (CR = 0.682). This result is probably due to the higher sensitivity of Cyt–Cit to the pH reduction over Cyt–Aco. The faster dissociation of the Cyt–Cit micelles in the endosome could lead to faster endosomal escape and diffusion into the cytoplasm.

In summary, we have developed an efficient method, which is based on charge-conversional PIC micelles, of protein delivery into cytoplasm. The stability of the PIC micelle under physiological salt conditions was significantly improved by increasing the charge density of the protein without any cross-linking. The charge conversion of the protein induced the efficient endosomal release, especially in the case of the PIC micelles containing Cyt–Cit. The long circulation time of the PIC micelles and controlled release activity of the charge-conversional moiety were combined in our charge-conversional PIC micelles, which could make them highly valuable for in vivo protein delivery. Moreover, when considering that the molecular weight of the PIC micelles is well over several megadaltons, these charge-conversional PIC micelles could potentially be optimal for the intracellular delivery of high-molecular-weight membrane-impermeable proteins.

Received: January 6, 2009
Published online: ■■ ■■, 2009

Keywords: charge conversion · cytochromes · drug delivery · endosomes · micelles

[1] I. M. Tomlinson, *Nat. Biotechnol.* **2004**, *22*, 521–522.
[2] a) K. Y. Lee, S. H. Yuk, *Prog. Polym. Sci.* **2007**, *32*, 669–697; b) N. W. S. Kam, Z. Liu, H. Dai, *Angew. Chem.* **2006**, *118*, 591–595; *Angew. Chem. Int. Ed.* **2006**, *45*, 577–581; c) I. I. Slowing, B. G. Trewyn, V. S. Y. Lin, *J. Am. Chem. Soc.* **2007**, *129*, 8845–8849.
[3] a) A. Harada, K. Kataoka, *Macromolecules* **1995**, *28*, 5294–5299; b) A. V. Kabanov, T. K. Bronich, V. A. Kabanov, K. Yu, A. Eisenberg, *Macromolecules* **1996**, *29*, 6797–6802; c) M. A.

Cohen Stuart, N. A. M. Besseling, R. G. Fokkink, *Langmuir* **1998**, *14*, 6846–6849.

[4] a) G. S. Kwon, K. Kataoka, *Adv. Drug Delivery Rev.* **1995**, *16*, 295–309; b) K. Kataoka, A. Harada, Y. Nagasaki, *Adv. Drug Delivery Rev.* **2001**, *47*, 113–131; c) M. Harada-Shiba, K. Yamauchi, A. Harada, I. Takamisawa, K. Shimokado, K. Kataoka, *Gene Ther.* **2002**, *9*, 407–414.

[5] a) K. Kataoka, H. Togawa, A. Harada, K. Yasugi, T. Matsumoto, S. Katayose, *Macromolecules* **1996**, *29*, 8556–8557; b) S. Katayose, K. Kataoka, *Bioconjugate Chem.* **1997**, *8*, 702–707; c) K. Itaka, N. Kanayama, N. Nishiyama, W. D. Jang, Y. Yamasaki, K. Nakamura, H. Kawaguchi, K. Kataoka, *J. Am. Chem. Soc.* **2004**, *126*, 13612–13613.

[6] a) A. Harada, K. Kataoka, *Macromolecules* **1998**, *31*, 288–294; b) A. Harada, K. Kataoka, *J. Am. Chem. Soc.* **1999**, *121*, 9241–9242; c) M. Jaturanpinyo, A. Harada, X. Yuan, K. Kataoka, *Bioconjugate Chem.* **2004**, *15*, 344–348.

[7] X. Yuan, Y. Yamasaki, A. Harada, K. Kataoka, *Polymer* **2005**, *46*, 7749–7758.

[8] a) J. K. Shetty, J. E. Kinsella, *Biochem. J.* **1980**, *191*, 269–272; b) Y. Lee, S. Fukushima, Y. Bae, S. Hiki, T. Ishii, K. Kataoka, *J. Am. Chem. Soc.* **2007**, *129*, 5362–5363; c) Y. Lee, K. Miyata, M. Oba, T. Ishii, S. Fukushima, M. Han, H. Koyama, N. Nishiyama, K. Kataoka, *Angew. Chem.* **2008**, *120*, 5241–5244; *Angew. Chem. Int. Ed.* **2008**, *47*, 5163–5166.

[9] N. Kanayama, S. Fukushima, N. Nishiyama, K. Itaka, W-D. Jang, K. Miyata, Y. Yamasaki, U-I. Chung, K. Kataoka, *ChemMedChem* **2006**, *1*, 439–444.

[10] K. Miyata, M. Oba, M. Nakanishi, S. Fukushima, Y. Yamasaki, H. Koyama, N. Nishiyama, K. Kataoka, *J. Am. Chem. Soc.* **2008**, *130*, 16287–16294.

[11] K. Masago, K. Itaka, N. Nishiyama, U. Chung, K. Kataoka, *Biomaterials* **2007**, *28*, 5169–5175.

[12] a) S. Kwon, J. H. Carson, *Anal. Biochem.* **1998**, *264*, 133–140; b) Y. Lee, H. Mo, H. Koo, J. Y. Park, M. Y. Cho, G. Jin, J. S. Park, *Bioconjugate Chem.* **2007**, *18*, 13–18; c) B. Z. Packard, A. Komoriya, D. D. Toptygin, L. Brand, *J. Phys. Chem. B* **1997**, *101*, 5070–5074.

[13] R. E. Childs, W. G. Bardsley, *Biochem. J.* **1975**, *145*, 93–103.

[14] S. Takae, K. Miyata, M. Oba, T. Ishii, N. Nishiyama, K. Itaka, Y. Yamasaki, H. Koyama, K. Kataoka, *J. Am. Chem. Soc.* **2008**, *130*, 6001–6009.

Communications

Protein Delivery

Y. Lee, T. Ishii, H. Cabral, H. J. Kim, J. Seo, N. Nishiyama, H. Oshima, K. Osada, K. Kataoka* ——— ■■■■–■■■■

Charge-Conversional Polyionic Complex Micelles—Efficient Nanocarriers for Protein Delivery into Cytoplasm

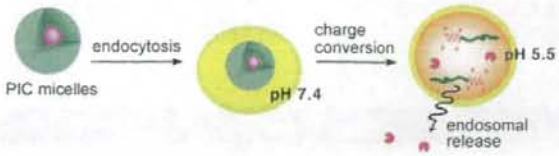

Special delivery! Polyionic complex (PIC) micelles that contain the charge-conversional moieties citaconic amide or *cis*-aconitic amide were developed for cytoplasmic protein delivery. The increase of the charge density on the protein cargo helped the stability of the PIC micelles without cross-linking, and the charge-conversion in endosomes induced the dissociation of the PIC micelles to result in efficient endosomal release (see picture).

10th Anniversary BioMACROMOLECULES

Article

Environment-Responsive Block Copolymer Micelles with a Disulfide Cross-Linked Core for Enhanced siRNA Delivery

Satoru Matsumoto, R. James Christie, Nobuhiro Nishiyama, Kanjiro Miyata, Atsushi Ishii, Makoto Oba, Hiroyuki Koyama, Yuichi Yamasaki, and Kazunori Kataoka

Biomacromolecules, **2009**, 10 (1), 119-127• DOI: 10.1021/bm800985e • Publication Date (Web): 05 December 2008

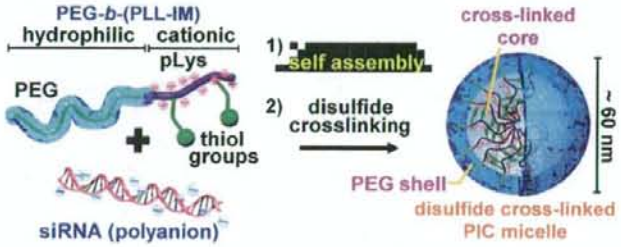

More About This Article

Additional resources and features associated with this article are available within the HTML version:

- Supporting Information
- Access to high resolution figures
- Links to articles and content related to this article
- Copyright permission to reproduce figures and/or text from this article

View the Full Text HTML

Environment-Responsive Block Copolymer Micelles with a Disulfide Cross-Linked Core for Enhanced siRNA Delivery

Satoru Matsumoto,[†] R. James Christie,[†] Nobuhiro Nishiyama,[§,⊥] Kanjiro Miyata,[‡,⊥] Atsushi Ishii,[†,#] Makoto Oba,[∥] Hiroyuki Koyama,[∥] Yuichi Yamasaki,[†,⊥] and Kazunori Kataoka*[,†,‡,§,⊥,▽]

Departments of Materials Engineering and Bioengineering, Graduate School of Engineering, Center for Disease Biology and Integrative Medicine and Department of Clinical Vascular Regeneration, Graduate School of Medicine, and Center for NanoBio Integration, The University of Tokyo, 7-3-1 Hongo, Bunkyo-ku, Tokyo, Japan, NanoCarrier Co., Ltd., 5-4-19 Kashiwanoha, Kashiwa, Chiba 277-0882, Japan, and CREST, Japan Science and Technology Agency, Japan

Received September 4, 2008; Revised Manuscript Received November 5, 2008

A core−shell-type polyion complex (PIC) micelle with a disulfide cross-linked core was prepared through the assembly of iminothiolane-modified poly(ethylene glycol)-*block*-poly(L-lysine) [PEG-*b*-(PLL-IM)] and siRNA at a characteristic optimum mixing ratio. The PIC micelles showed a spherical shape of ~60 nm in diameter with a narrow distribution. The micellar structure was maintained at physiological ionic strength but was disrupted under reductive conditions because of the cleavage of disulfide cross-links, which is desirable for siRNA release in the intracellular reductive environment. Importantly, environment-responsive PIC micelles achieved 100-fold higher siRNA transfection efficacy compared with non-cross-linked PICs prepared from PEG-*b*-poly(L-lysine), which were not stable at physiological ionic strength. PICs formed with PEG-*b*-(PLL-IM) at nonoptimum ratios did not assemble into micellar structure and did not achieve gene silencing following siRNA transfection. These findings show the feasibility of core cross-linked PIC micelles as carriers for therapeutic siRNA and show that stable micellar structure is critical for effective siRNA delivery into target cells.

Introduction

siRNA is a 19−21 base-paired double-stranded RNA that plays a key role in the post-transcriptional gene silencing phenomenon called RNA interference, or RNAi.[1,2] Because siRNAs induce highly efficient gene silencing at the translation level, many efforts have been undertaken to transform their use from a research tool to a therapeutic agent.[3] A reason for the excitement of RNAi therapies is that the therapeutic target (mRNA) resides in the cell cytoplasm, and thus the nuclear membrane is not an obstacle as in DNA-based therapies. Some studies have already progressed to clinical trials, but almost all cases utilize local administration, an application limited to readily accessible tissues such as those found in the ocular and respiratory systems.[4] Despite great promises of therapeutic potential, many obstacles currently prevent systemic application of siRNA. For example, siRNAs are known to degrade rapidly into noneffective fragments in the RNase-rich physiological environment. Additionally, systemically administered naked siRNAs are rapidly eliminated from circulation, with plasma half lives reported to be as short as 0.03 h in mice[5] and 0.1 h in rats.[6] It is clear that an innovative carrier system for systemic administration is required for further development of siRNA as a universal drug. Fundamental design and evaluation of an siRNA carrier, which could be developed into a system for therapeutic use, was the specific aim of this work.

Recently, a number of polyion complexes (PICs) formed through electrostatic interaction between anionic siRNA and cationic polymers have been investigated as carriers of therapeutic siRNA. For example, polyethylenimine (PEI) is a well known cationic polymer that is capable of transfecting nucleic acids.[7] However, the majority of intravenously administered PEI/nucleic acid complexes seem to undergo entrapment by pulmonary capillary beds, resulting in rapid clearance from circulation.[8,9] Modification of PEI with poly(ethylene glycol) (PEG),[10,11] targeting ligand, or both was examined as a method for improving the pharmacokinetics (PK) of PICs because PEGylation of drug carriers generally prolongs blood circulation time and certain ligands direct carriers to target tissues. Although the ligand-installed PEGylated PEI/siRNA complex demonstrated remarkable antitumor effects, no significant extension in the circulation time of siRNA in the blood stream was observed, and eventually, a considerable amount of the injected PIC was unfavorably distributed to nontarget organs such as the liver, lungs, and spleen.[11] Alternatively, PEGylated PICs have been prepared through electrostatic interaction between PEG-*block*-polycation copolymers and nucleic acids such as plasmid DNA or antisense oligo-DNA and are termed PIC micelles because of a core−shell structure with the core surrounded by a dense PEG corona.[12,13] These PIC micelles demonstrate remarkable properties as delivery vehicles for DNA: excellent colloidal stability in proteinaceous media, protection of incorporated DNA against enzymatic degradation, and prolonged blood circulation.[14,15] Hence, PIC micelles have been

* Corresponding author. Tel: +81-3-5841-7138. Fax: +81-3-5841-7139. E-mail: kataoka@bmw.t.u-tokyo.ac.jp.
† Department of Materials Engineering, Graduate School of Engineering, The University of Tokyo.
‡ Department of Bioengineering, Graduate School of Engineering, The University of Tokyo.
§ Center for Disease Biology and Integrative Medicine, Graduate School of Medicine, The University of Tokyo.
∥ Department of Clinical Vascular Regeneration, Graduate School of Medicine, The University of Tokyo.
⊥ Center for NanoBio Integration, The University of Tokyo.
NanoCarrier Co., Ltd.
▽ Japan Science and Technology Agency.

10.1021/bm800985e CCC: $40.75
Published on Web 12/05/2008

considered to be siRNA carriers,[16] but little is known, particularly from a physicochemical viewpoint, about the process of PIC micelle formation from flexible PEG-based block cationers and short and rigid siRNAs. Recently, a 14 Lys-PEG (K_{14}-PEG) linear diblock copolymer and siRNA were shown to achieve monomolecular assembly but not the multimolecular assembly that is necessary for PIC micelle formation.[17] In this work, we investigated the formation of PIC micelles incorporating siRNA within the core with hopes of shedding light on the factors affecting the assembly, stability, and efficacy of this novel type of siRNA carrier as a fundamental step in the development of effective PIC-based siRNA delivery systems.

It is assumed that siRNA is more difficult to incorporate in PIC micelle structures than plasmid DNA and oligo-DNA because siRNA is $<^1/_{100}$ the length of plasmid DNA and has more restricted conformational freedom than single-stranded oligo-DNA. Therefore, structural refinement of the polycations used for complexation may improve micelle formation and stability for delivery systems of short and rigid siRNA. Whereas increased stability in biological milieu is needed to allow PIC micelles to reach their target, PIC micelles are also required to release siRNA promptly in the cytoplasm of the target cell for recruitment of siRNA into RNAi machinery. Thus, ideal PIC micelles for siRNA delivery must meet the following rather conflicting requirements: stability of PIC micelles in extracellular media with efficient release of free siRNA from their interior to the cytoplasm of target cells.

In our previous study, poly(ethylene glycol)-*block*-poly(L-lysine) (PEG-*b*-PLL) copolymers were modified to contain thiol groups using *N*-succinimidyl 3-(2-pyridyldithio)propionate (SPDP) to construct PIC micelles with a disulfide cross-linked core for the delivery of plasmid DNA and antisense oligo-DNA.[18−21] The disulfide cross-links are stable under nonreductive physiological conditions contributing to the maintenance of micellar structure and then cleave under reductive conditions following cellular uptake. Disulfides are expected to cleave in the cytoplasm because of elevated levels of glutathione (50−1000 times higher than that in extracellular media[22]). Hence, PIC micelles containing disulfide cross-links within the core may provide the needed stability tradeoff: increased stability in extracellular environment and prompt release of cargo molecules inside the target cell through the cleavage of disulfide bonds. Indeed, plasmid-DNA-loaded PIC micelles comprising a disulfide cross-linked core showed appreciable gene expression in the liver after intravenous administration to mice.[21]

Here we report a novel micellar system for siRNA delivery on the basis of the strategy of core cross-linking via disulfide formation to exert selective release of free siRNA in intracellular milieu while protecting siRNA in extracellular milieu from degradation and nonspecific clearance. PEG-*b*-PLL copolymer was reacted with 2-iminothiolane to obtain poly(ethylene glycol)-*block*-poly[L-*N*-(1-imino-4-mercaptobutyl)lysine] [PEG-*b*-(PLL-IM)] with a portion of lysine residues bearing both mercaptopropyl and amidine groups. This thiolated copolymer was subsequently used to prepare disulfide cross-linked PIC micelles incorporating siRNA. The combination of disulfide cross-links and cationic amidine groups were found to contribute to the increase in the stability of the micelles. Importantly, PIC micelles from PEG-*b*-(PLL-IM) achieved 100-fold higher siRNA activity compared with those from unmodified PEG-*b*-PLL. Such remarkable siRNA activity was correlated with the formation of core−shell-type PIC micelles at critical mixing ratios of block copolymers and siRNA.

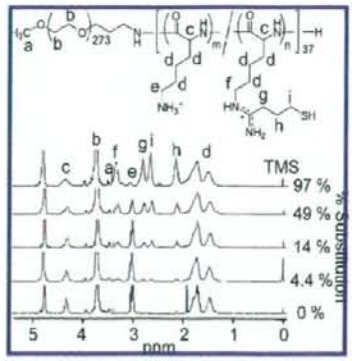

Figure 1. ^{1}H NMR spectra of PEG-*b*-(PLL-IM). Solvent, D_2O; temperature, 25 °C; concentration, 10 mg/mL.

Materials and Methods

Reagents. Dimethyl sulfoxide (DMSO), diethyl ether, dithiothreitol (DTT), D_2O, LiCl, and 2-iminothiolane were purchased from Wako Pure Chemical Industries (Osaka, Japan). Dulbecco's modified Eagle's medium (DMEM), *N*,*N*-diisopropylethylamine (DIPEA) and *N*-methylpyrrolidone (NMP) were purchased from Sigma-Aldrich (St. Louis, MO). Dual-luciferase reporter assay system and pGL3-control and pRL-CMV vectors were purchased from Promega (Madison, WI). Hoechst 33342 was obtained from Dojindo Laboratories (Kumamoto, Japan). SYBR Green II was purchased from Takara Bio (Shiga, Japan). Lipofectamine2000 was purchased from Invitrogen (Carlsbad, CA). siRNA and Cy5-labeled siRNA were synthesized by Dharmacon (Lafayette, CO) and Nihon Bioservice (Saitama, Japan), respectively. The sequences of siRNA against *Photinus pyralis* luciferase were as follows: sense 5′-CUUACGCUGAGUACUUCGAdTdT-3′, antisense 5′-UCGAAGUACUCAGCGUAAGdTdT-3′.

Synthesis of PEG-*b*-(PLL-IM). PEG-*b*-PLL copolymer (M_w of PEG: 12 000; polymerization degree of PLL: 37; M_w/M_n: 1.08) was synthesized as previously described.[20,23] Iminothiolane modification of PEG-*b*-PLL was achieved by reacting primary amino groups in side chains of PLL segments with 2-iminothiolane. First, PEG-*b*-PLL (37.5 mg/mL) and 2-iminothiolane (25 mg/mL) were separately dissolved in NMP containing 5 wt % LiCl. Then, the solutions were mixed at various molar ratios of 2-iminothiolane/Lys up to 2.0 and stirred at 25 °C for 18 h after the addition of DIPEA (5 equiv relative to lysine (Lys) units). The mixtures were purified by precipitation in a 15-fold excess of diethyl ether (60 mL). Precipitated polymer was redissolved in 0.01 N HCl (20 mL), dialyzed against distilled water (MWCO: 2000), and lyophilized to obtain pure PEG-*b*-(PLL-IM) copolymer. The products were subjected to ^{1}H NMR analysis in D_2O using a 300 MHz spectrometer (EX 300, JEOL, Tokyo, Japan). The degree of substitution for each PEG-*b*-(PLL-IM) was determined from the ^{1}H NMR spectra shown in Figure 1 by the peak intensity ratio of the β-, γ-, and δ-methylene protons of Lys ($(CH_2)_3$, $\delta = 1.3$ to 1.9) to the protons of trimethylene units of mercaptopropyl groups ($HS-(CH_2)_3$, $\delta = 2.1$ to 2.8). The calculated substitution degrees are shown as PEG-*b*-(PLL-$IM_{x\%}$) where x stands for the percent substitution.

Preparation of Disulfide Cross-Linked Polyion Complex Systems. Before complexation with siRNA, PEG-*b*-(PLL-IM) solutions were incubated in a DTT solution (100 mM in 10 mM HEPES−NaOH, pH 7.4) at 25 °C for 30 min to reduce any disulfide bonds. Then, polymer solution was added to a two-fold excess volume of 15 μM siRNA (600 mM phosphate groups of siRNA) solution at different mixing ratios to form PICs. The mixing ratio for each complexation study was determined by N/P: [primary amines and amidines of block copolymers]/[phosphate groups of siRNA]. After overnight incubation at 25 °C, thiol groups were oxidized to form disulfide cross-links by dialysis against 10 mM HEPES−NaOH buffer (pH 7.4) containing 0.5%

DMSO at 37 °C for 2 days, followed by 2 days of additional dialysis against 10 mM HEPES−NaOH buffer (pH 7.4) for the removal of DMSO. To confirm oxidation, remaining free thiol groups were quantified using Ellman's method.[24]

Measurement of Scattered Light Intensity, Size, and ζ Potential of Polyion Complexes. PICs formed from PEG-*b*-(PLL-IM) and siRNA were evaluated by static (SLI) and dynamic (DLS) light scattering measurements before and after the removal of DTT from the complexation milieu: the former measurement was carried out to examine the effect of the mixing ratios on the formation of PIC assemblies, whereas the latter measurement was aimed to evaluate the stability and environment responsiveness of the disulfide cross-linked systems. All light scattering measurements were carried out using a Zetasizer Nano ZS (Malvern Instruments, Malvern, UK) equipped with a He−Ne laser (λ = 633 nm) as the incident beam. In DLS measurements, size distributions were determined by cumulant and histogram analysis, and results are shown as the z-average size (cumulant mean) with polydispersity index (PDI) (defined in the ISO standard document 13 321:1996) and the histogram of size distribution. Briefly, cumulant analysis was performed by expanding the logarithm of the normalized correlation function $g^{(1)}(t)$ as a power series in the time t

$$\ln[g^{(1)}(t)] = -K_1 t + (1/2)K_2 t^2 + \ldots$$

yielding an average of the reciprocal relaxation time, K_1, and PDI, K_2/K_1^2. K_1 was further converted to a translational diffusion coefficient to calculate the z average by using the Stokes−Einstein equation. The ζ potentials of the complexes were measured in 10 mM HEPES−NaOH buffer (pH 7.4) containing 150 mM NaCl at 37 °C. All samples were equilibrated to the defined temperature for 24 h prior to measurement.

Gel Retardation Analysis. Non-cross-linked PICs prepared in reductive milieu as described above were electrophoresed at 100 V for 1 h on 20% polyacrylamide gel in tris-borate EDTA buffer (100 mM Tris, 90 mM boric acid, 1 mM EDTA) to qualitatively determine if free siRNA remained after polymer complexation. The gel was stained with SYBR Green II according to the manufacturer's protocol and visualized using a UV transilluminator.

Stability of Polyion Complexes. The effect of cross-linking on PIC stability was determined as a function of NaCl concentration using a Zetasizer Nano ZS (Malvern Instruments, Malvern, UK). The assay was performed by measuring the scattering light intensity (SLI) of PICs after 24 h of incubation at 37 °C in solutions containing different NaCl concentrations ranging from 75 to 600 mM NaCl. PIC size distribution was also obtained by histogram analysis of DLS measurement.

Atomic Force Microscopy Analysis. Disulfide cross-linked PIC assemblies were visualized by AFM imaging. For each analysis, sample solution (4 μL) was deposited onto a freshly cleaved mica substrate for 30 s, and the solution was dried under a gentle flow of nitrogen. AFM imaging was performed in tapping mode with standard silicon probes (125 μm in length, Veeco Instruments, CA) on a nanoscope (Veeco Instruments). The cantilever oscillation frequency was tuned to the resonance frequency of the cantilever, 200−400 kHz. Raw AFM images have been processed for only background removal (flattening) using the microscope manufacturer's image-processing software.

siRNA Transfection. Huh7 cells (human hepatoma cells) were plated onto 24-well culture plates (2×10^4 cells/well), followed by 20 h of incubation in DMEM containing 10% fetal bovine serum (FBS). Then, 360 ng/well pGL3-control, encoding *Photinus pyralis* luciferase (Pp-Luc), and 40 ng/well pRL-CMV, encoding *Renilla reniformis* luciferase (Rr-Luc), plasmid DNA were applied with Lipofectamine2000 according to the manufacturer's instructions, and cells were further incubated for 4 h to allow transfection of plasmid DNAs. The medium was replaced, and PICs with or without disulfide cross-linking were applied to each well for transfection of siRNA (1−500 nM) against Pp-Luc. After 48 h, cells were rinsed with PBS and subjected to a luciferase expression assay using the dual-luciferase reporter assay system. For each assay, Pp-Luc and Rr-Luc luminescence was measured using a Mithras LB940 plate reader (Berthold Technologies, Bad Wildbad, Germany) after the addition of appropriate substrates. Pp-Luc activities were normalized by Rr-Luc activities, and values are expressed as a ratio to the control value (mean ± SD, n = 4).

Flow Cytometry. Huh7 cells were plated onto six-well culture plates, followed by 24 h of incubation in DMEM containing 10% FBS. The medium was replaced, and Cy5-siRNA-incorporated PICs with or without disulfide cross-linking were applied (100 nM siRNA) to each well. After 1 h, cells were rinsed three times with PBS and collected by trypsinization. The collected cells were centrifuged at 100*g* for 2 min and resuspended in PBS. The fluorescence intensity was detected and acquired using a BD LSR II instrument (BD Biosciences, Franklin Lakes, NJ) equipped with FACS Diva software (BD Biosciences). Detection of Cy5 fluorescence was achieved using a 633 nm He−Ne laser for excitation, and a 660/20 band-pass filter for emission.

Confocal Laser Scanning Microscopy. Huh7 cells were seeded onto 35 mm glass-bottomed Petri dishes, followed by 24 h of incubation in DMEM containing 10% FBS. The medium was replaced, and Cy5-siRNA-incorporated PICs with or without disulfide cross-linking were applied at 100 nM siRNA to each dish. After 3 h, cells were stained with Hoechst 33342 according to the manufacturer's protocol and were then rinsed three times with PBS and observed by confocal laser scanning microscopy (CLSM) under fresh culture medium. CLSM observation was performed using a LSM 510 (Carl Zeiss, Oberkochen, Germany) microscope equipped with a 63× objective (C-Apochromat, Carl Zeiss). Detection of Cy5 and Hoechst 33342 fluorescence was achieved using 633 nm He−Ne and 710 nm Mai Tai lasers for excitation, and 651−704 nm and 390−465 nm band-pass filters for emission, respectively.

Results

Preparation of PEG-*b*-(PLL-IM). Primary amines in lysine residues of PEG-*b*-PLL readily reacted with the cyclic imidoester 2-iminothiolane via a ring-opening reaction, generating mercaptopropyl groups through amidine bonds to obtain PEG-*b*-(PLL-IM).[25] In ^{1}H NMR measurements, the transformation of primary amines to amidines was evident: the ε-methylene protons of lysine residues were shifted downfield (e to f, Figure 1) in addition to the appearance of proton signals characteristic to the CH_2 units of γ-mercapto-propyl groups (g−i, Figure 1). The degree of substitution was calculated from these characteristic signals, as described in the Materials and Methods section. By changing the feed ratios of 2-iminothiolane to primary amino groups of PEG-*b*-PLL, a series of PEG-*b*-(PLL-IM) with varying degrees of substitution was obtained in good yield (71−90%). The reactions at feed ratios (2-iminothiolane/primary amine) of 0.15, 0.6, 1, and 2 resulted in 14, 48, 69, and 97% substitutions, respectively.

Formation of Polyion Complexes from PEG-*b*-(PLL-IM) and siRNA. PEG-*b*-(PLL-IM) copolymer solutions were mixed with siRNA at varying N/P ratios under reductive conditions to form the desired PICs. PIC formation was confirmed by the observation of increased scattered light intensity (SLI), which is correlated to the product of molar concentration and squared molecular weight of the analytes. Of interest, the SLI of each PIC solution reached a maximum at a specific N/P ratio, which varied depending on the substitution degree of PEG-*b*-(PLL-IM) (Figure 2). For example, the PEG-*b*-PLL system showed a maximum SLI at N/P = 1.2, and a subtle change in N/P induced a drastic decrease in the SLI, indicating that PICs formed from PEG-*b*-PLL assembled into higher ordered micelle structures only at N/P = 1.2. Likewise, a critical N/P ratio for the formation of higher order large PIC assemblies was found for each PEG-*b*-(PLL-IM) except for PEG-*b*-(PLL-IM$_{97\%}$), in which the SLI continuously increased to N/P = 7.

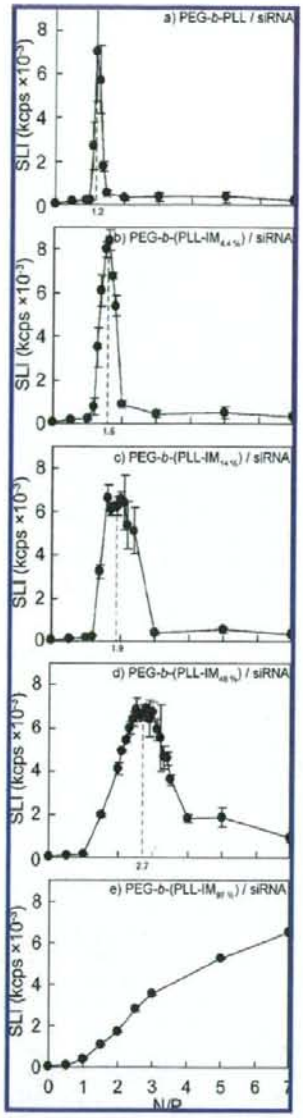

Figure 2. Static light scattering analysis of PIC assemblies formed from PEG-*b*-(PLL-IM)s and siRNA at various N/P ratios under reductive conditions. Scattered light intensity (SLI) was recorded at 25 °C in 10 mM HEPES−NaOH buffer (pH 7.4) containing 33 mM DTT. Values are expressed as the mean ± SD, $n = 3$.

The size distributions of the PICs formed at the characteristic N/P ratio that gives a maximum SLI in Figure 2 were analyzed by DLS. Curiously, the autocorrelation curve of PIC assemblies formed from PEG-*b*-PLL and siRNA exhibited complicated and slow decay that was out of the range of particle size analysis by DLS (data not shown). The PEG-*b*-PLL system might not form a simple spherical micellar structure as suggested in the result of histogram analysis (Figure 3a). In contrast, PIC assemblies formed from siRNA and PEG-*b*-(PLL-IM) with >14% substitution showed narrow size distributions with PDI < 0.045 and diameters ranging from 40 to 58 nm, depending

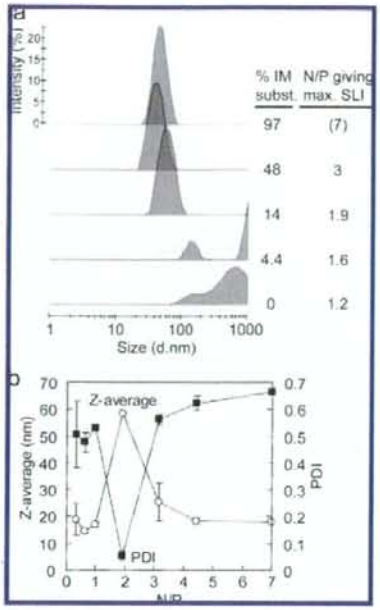

Figure 3. Dynamic light scattering analysis of PIC assemblies formed from PEG-*b*-(PLL-IM) and siRNA under reductive conditions. (a) Size distributions of the PIC assemblies formed at the N/P ratio of each maximum of SLI. (b) N/P dependency of size distributions of the complexes formed from PEG-*b*-(PLL-IM$_{14\%}$) and siRNA. All measurements were performed at 25 °C in 10 mM HEPES−NaOH buffer (pH 7.4) supplemented with 33 mM DTT.

on the substitution degree (Figure 3a and Supporting Information). These size and PDI values are consistent with the formation of spherical micelles with core−shell architecture in which the PIC core of siRNA and PLL-IM is surrounded by a PEG shell. Note that even for PEG-*b*-(PLL-IM)s, a deviation in the N/P ratios from the critical value resulted in a significant increase in PDI values accompanied by decreased SLI, which suggests a transformation to less-ordered micelle structures with a lower association number. A typical N/P dependency of PDI and size distribution for PICs formed from PEG-*b*-(PLL-IM$_{14\%}$) and siRNA is shown in Figure 3b, indicating that narrowly distributed PIC micelles with a size that was consistent with the core−shell model were formed only at the characteristic point (N/P = 1.9) where the SLI also showed a maximum value (Figure 2).

The incorporation of siRNA into PIC assemblies was confirmed by polyacrylamide gel electrophoresis (Figure 4). Interestingly, free siRNA was not observed above the critical N/P mixing ratios shown in Figure 2 for all of the samples with 0 to 69% substitution degree, indicating the stable association of siRNA into PICs above the critical N/P ratio but not organized micelle structures as the SLI decreased substantially. As for the sample with 97% substitution degree [PEG-*b*-(PLL-IM$_{97\%}$)], a migrative fraction of siRNA could not be detected above the N/P ratio of 4.

Characterization of Disulfide Cross-Linked Polyion Complex Assemblies. Multimolecular PIC assemblies, defined as PIC micelles, formed from siRNA and PEG-*b*-(PLL-IM) prepared at the critical N/P ratio under reductive conditions were subsequently dialyzed against 10 mM HEPES−NaOH buffer (pH 7.4) containing 0.5% DMSO to form disulfide cross-links

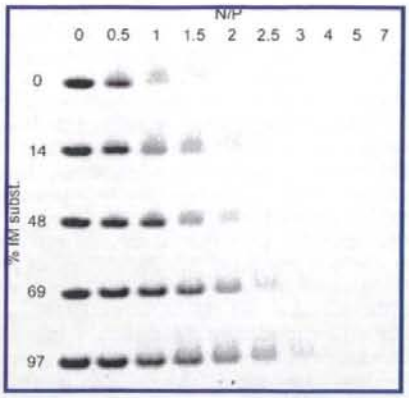

Figure 4. Gel retardation analysis of siRNA complexed with PEG-*b*-(PLL-IM)s under reductive conditions. Free siRNA was stained with SYBR Green II and visualized using a UV transilluminator.

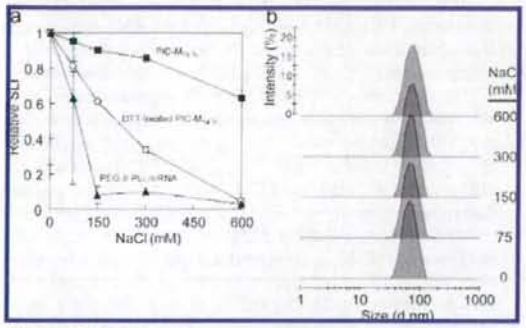

Figure 5. Stability and environment responsiveness of disulfide cross-linked micelles. (a) Scattered light intensity of PIC-$M_{14\%}$, DTT-treated PIC-$M_{14\%}$, and PIC assemblies from PEG-*b*-(PLL)/siRNA with increased concentration of NaCl. (b) Size distributions of PIC-$M_{14\%}$ at each NaCl concentration.

through the oxidation of thiol groups. After dialysis, the amount of residual thiol groups was determined to be <10% of the initial value for all of the samples, indicating that the core of the PIC-Ms were successfully cross-linked through disulfide bonds. (See the Supporting Information.) Hereafter, siRNA-incorporated PIC micelles prepared from PEG-*b*-(PLL-$IM_{x\%}$) are abbreviated as PIC-$M_{x\%}$.

The stability of PIC assemblies against ionic strength was evaluated by SLI and DLS measurements at various NaCl concentrations. As seen in Figure 5a, there was a significant decrease in SLI for the PEG-*b*-PLL/siRNA system with an increase in NaCl concentration, indicating that the system is highly sensitive to ionic strength, and cannot tolerate physiological salt concentration. Alternatively, PIC-$M_{14\%}$ cross-linked micelles retained >80% of their initial SLI value at 300 mM NaCl and retained 60% of their initial SLI value even at a NaCl concentration as high as 600 mM. Cumulant analysis of DLS measurements at various NaCl concentrations revealed that the PIC-$M_{14\%}$ maintained an almost constant diameter (~70 nm by z average) with very narrow distribution (PDI < 0.067) up to 600 mM NaCl. (See the Supporting Information.) Histogram analysis of DLS measurement further corroborated the stable and narrow size distribution of PIC-$M_{14\%}$ against an increase in NaCl concentration, as shown in Figure 5b.

Table 1. ζ Potentials of Disulfide Cross-Linked Micelles

% IM subst.	N/P giving max SLI	ζ potential (mV) (mean ± SD)
0	1.2	−2.6 ± 1.3
4.4	1.6	−0.73 ± 0.44
14	1.9	−2.4 ± 1.1
49	3	−1.4 ± 2.1
69	3.9	−0.73 ± 0.15

The stability of PIC-$M_{14\%}$ at different NaCl concentrations was also evaluated by SLI after the addition of DTT, which aimed to cleave disulfide cross-linking in the core and disrupt micelle stability. As seen in Figure 5a, the addition of DTT to PIC-$M_{14\%}$ solution induced a significant decrease in the SLI with increasing NaCl concentration (Figure 5a, ○). This result indicates the critical role of disulfide cross-links in the improved stability of PIC micelles against increased ionic strength as well as the feasibility of dissociation of cross-linked micelles under reductive conditions and physiological ionic strength, such as the intracellular environment.

Table 1 shows the ζ potential of PIC-$M_{x\%}$ formed at the critical N/P ratio depending on the substitution degree in 10 mM HEPES−NaOH (pH 7.4) containing 150 mM NaCl at 37 °C. Data for a PEG-*b*-PLL/siRNA system formed at the critical N/P ratio of 1.2 are also shown as a control. The ζ potential varied only slightly from −2.6 to −0.73 mV, regardless of micelle composition. Furthermore, these small absolute values of ζ potential remained unchanged even after the storage of cross-linked PIC-Ms in solution for several months. (See the Supporting Information.) The stable and electrostatically neutralized PIC-Ms in the stored solution are consistent with the formation of a core−shell structure where the PEG shell prevents micelle aggregation through decreased interfacial free energy as well as increased steric repulsion.

The morphology of PIC assemblies was directly observed by AFM, as shown in Figure 6. PIC-$M_{48\%}$ had a spherical shape with a diameter of ~50 nm, which is consistent with the formation of polymeric micelles. There was no change in the size and morphology even after incubation in medium containing 150 mM NaCl. Taken together with the data from light scattering analyses, it is reasonable to conclude that a stable disulfide cross-linked PIC micelle was formed from PEG-*b*-(PLL-IM)s and siRNA at the N/P ratio coinciding with maximum SLI intensity.

siRNA Transfection Using Disulfide Cross-Linked Micelles. A series of disulfide cross-linked micelles composed of PEG-*b*-(PLL-IM) with various substitution degrees, PIC-$M_{x\%}$, were evaluated as carriers for siRNA in cultured cells. In this experiment, Huh7 cells were transiently transfected with the reporter genes Pp-Luc and Rr-Luc, followed by the treatment with PIC-$M_{x\%}$ prepared at the appropriate N/P ratio containing siRNA against Pp-Luc. After a transfection period of 48 h, the inhibition of Pp-Luc expression was evaluated by measuring the relative expression of Pp-Luc/Rr-Luc. First, we examined the siRNA transfection efficacy of disulfide cross-linked micelles formed from PEG-*b*-(PLL-IM) with different substitution degrees (PIC-$M_{x\%}$) at a concentration of 100 nM siRNA. Ultimately, PIC-$M_{14\%}$ was found to achieve the highest silencing efficacy of Pp-Luc gene (Figure 7a). The system with higher and lower substitution degrees than PIC-$M_{14\%}$ resulted in lower siRNA transfection efficacy. We then evaluated the dose-dependent siRNA transfection efficiencies of PIC-$M_{14\%}$ in comparison with naked siRNA and non-cross-linked PIC assemblies from PEG-*b*-PLL as controls. PIC-$M_{14\%}$ had an ED_{50} (defined as the siRNA concentration required to induce 50% of

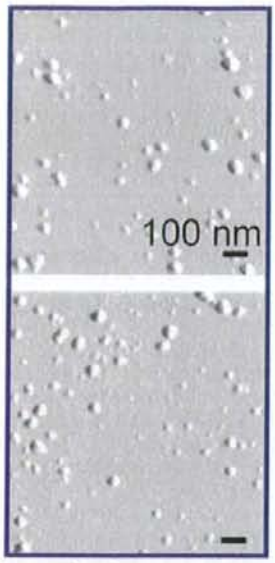

Figure 6. AFM images of disulfide cross-linked micelles (PIC-$M_{48\%}$). Images were acquired before (upper) and after (lower) incubation in 150 mM NaCl.

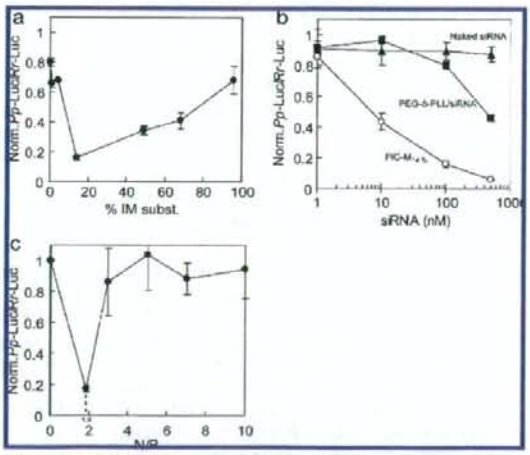

Figure 7. Disulfide cross-linked micelle-mediated siRNA transfection. (a) 100 nM siRNA was transfected in Huh7 cells with disulfide cross-linked micelles. Each of the micelles was prepared from PEG-*b*-(PLL-IM) and siRNA at the optimal N/P maximum in SLI. (b) Dose-dependent knockdown by PIC-$M_{14\%}$ compared with naked siRNA and non-cross-linked PIC assemblies from PEG-*b*-PLL and siRNA. (c) N/P dependency of the knockdown efficiency of the disulfide cross-linked complexes formed from PEG-*b*-(PLL-$IM_{14\%}$) and siRNA. Values are expressed as the mean ± SD, $n = 4$.

gene knockdown) that was approximately two orders of magnitude lower than that of PIC assemblies of PEG-*b*-PLL, which indicates a significant improvement in siRNA transfection efficacy by the introduction of disulfide cross-links to the PIC-M structure (Figure 7b). The effect of N/P ratios used to form cross-linked assemblies from PEG-*b*-(PLL-$IM_{14\%}$) on siRNA transfection efficacy was also evaluated. As shown in Figure 7c, effective siRNA transfection was achieved at only the critical N/P ratio of 1.9, where the PIC assembled in the micellar structure, as seen in Figures 2 and 3b. Apparently, the formation of micellar structure is well correlated with siRNA transfection efficiency. The siRNA transfection efficacy of Lipofectamine2000 was also determined using the dual luciferase assay for comparison with micellar systems. A significant decrease in Pp-Luc (Pp-Luc/Rr-Luc = 0.03 at 100 nM siRNA) was accompanied by a significant decrease in Rr-Luc expression (>80% lower expression than micellar systems), which indicated Lipofectamine2000 cytotoxicity. (See the Supporting Information.) The cytotoxicity of Lipofectamine2000 prevented a direct comparison with micellar systems under the conditions of this reporter system. Micellar systems showed minimal cytotoxicity at all concentrations used for dual luciferase assay with >75% viability retained at 100 nM siRNA for PIC-$M_{14\%}$. (See the Supporting Information.) Although little is known about the biocompatibility of iminothiolane functional groups, the observed low cytotoxicity in cultured cells is promising and warrants further investigation in vivo to determine the biocompatibility and tolerance of these micellar siRNA delivery systems.

To investigate the transfection properties of PIC micelles in more detail, PICs containing Cy5-labeled siRNA were prepared and applied to Huh7 cells. It should be noted that the incorporation of Cy5-labeled siRNA into micelles resulted in ~75% fluorescence quenching, with no significant shift in absorbance or emission maximum. (See the Supporting Information.) Figure 8a shows flow cytometric analysis (FCM) of Huh7 cells treated with PIC-$M_{14\%}$ and PIC assemblies from PEG-*b*-PLL. We analyzed FCM data by determining the mean fluorescence intensity (MFI) of the cell population. Significantly higher fluorescence (MFI = 5221) was observed for Cy5-siRNA incorporated PIC-$M_{14\%}$ compared with the PIC assembly formed from PEG-*b*-PLL/Cy5-siRNA (MFI = 632) and naked Cy5-siRNA (MFI = 1032). The uptake of free siRNA may appear to be higher than expected because of Cy5 quenching in micelle cores and the presence of hydrophobic dye that may facilitate interaction with cell membrane components and increase uptake. It should be noted that the absolute values of fluorescence intensity are relatively low for all three species, indicating that cellular uptake was not rapid. CLSM of cells treated with PIC micelles containing Cy5-siRNA further supported the data of FCM analysis, as seen in Figure 8b. Whereas the fluorescence of naked Cy5-siRNA or Cy5-siRNA transfected with PEG-*b*-PLL was hardly detectable under the same CLSM configuration as that used for PIC-$M_{14\%}$, 100% of cells transfected with PIC-$M_{14\%}$ gave CLSM images with an intracellular localization of Cy5 fluorescence signal 3 h after transfection. These results demonstrate that the highly efficient knockdown of the Pp-Luc gene by PIC-$M_{14\%}$ was achieved by an effective uptake of siRNA in the cell presumably due to the formation of a stable micellar structure.

Discussion

In this study, we have demonstrated that disulfide cross-linked PIC-Ms appreciably enhanced siRNA transfection. Stable and unimodal micellar formation occurred at a specific mixing ratio (N/P) only when the primary amino groups of PEG-*b*-PLL were at least partially modified with thiol groups through amidine bonds. These disulfide cross-linked micelles exhibited remarkable stability in physiological medium, underwent dissolution upon the reduction of disulfide cross-links to allow the release of entrapped siRNA, and achieved 100 times higher transfection efficiency than PIC assemblies without disulfide cross-links.

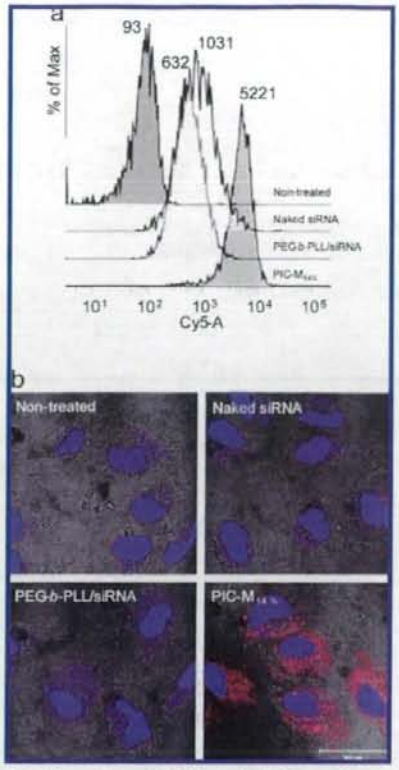

Figure 8. Cellular uptake of Cy5-labeled siRNA transfected with PIC-$M_{14\%}$ or assemblies formed from PEG-*b*-PLL at the N/P of maximum in SLI. (a) Flow cytometric analysis of Huh7 cells 1 h after Cy5-siRNA transfection. Values indicate the mean fluorescence intensity (MFI) of the cell population. Nontreated represents the fluorescence emitted from untreated Huh7 cells. (b) Confocal laser scanning microscopic analysis of Huh7 cells 3 h after Cy5-siRNA (red) transfection. Cell nuclei were stained with Hoechst 33342 (blue).

The assembly of block catiomers and siRNA showed a distinct change in association number governed by the mixing ratio (N/P). The relatively weak SLI obtained from mixed solutions of block catiomer and siRNA at ratios of N/P ≤ 1 indicated that few recognizable multimolecular assemblies with increased association number formed (Figure 2). Considering the gradual decrease in the migrative siRNA fraction in PAGE analysis (Figure 4) as well as the moderate SLI when N/P was increased by 1, siRNA excess mixtures might have formed charge−stoichiometric complexes that do not assemble into micelle-like multimolecular assembly. However, at the very specific N/P typically slightly above 1, SLI showed a dramatic increase, suggesting the successful formation of multimolecular assemblies. Although, possibly due to incomplete protonation of PEG-*b*-PLL lysines ($pK_a \approx 9.5$, ~95% protonation at pH 7.3),[23,26] N/P maxima did not precisely correspond to the equal charge ratios of siRNA and block catiomer; controlled excess of catiomer appeared to be crucial for micellar assembly. A likely explanation of the mechanism of this distinct assembling behavior is that a slight excess amount of block catiomers assists multimolecular assembly through intermolecular ion bridging. It should be noted that multimolecular assembly was abrogated with a further increase in N/P, as seen by the steep decrease in SLI and increase in PDI (Figures 2 and 3b), even though stable complexation of block catiomer and siRNA was strongly suggested by the absence of migrative siRNA upon gel electrophoresis of samples prepared above the characteristic N/P that gives maximum SLI (Figure 4). In the block catiomer−large excess mixture, the multimolecular assembly could have been hindered by the electrostatic repulsion between catiomer−excess small complexes or steric inconsistency, which is characteristic of block copolymers, as previously described.[27]

Recent experiments with PEGylated polyelectrolyte systems containing PEG-*block*-poly(aspartate) (PEG-*b*-PAsp), PEG-*b*-PLL, and PLL show that assembly behavior is influenced by a variety of factors including polyion chain length and the presence of homopolymer.[27] This study demonstrated that block copolymer acts as the host molecule in PICs and that PEGylation of polyions may change the complexation process from loose noncooperative association to tight cooperative pairing, in turn leading to growth into stoichiometric core−shell PIC micelles with an appreciably high association number.

In the study described above, light scattering intensity increased to an optimum upon mixing of PEG-*b*-PAsp with increasing ratios of PLL, whereas the size underwent a sharp drop in the region with excess PLL because in this range, all PEG-*b*-PAsp chains behave as host molecules to participate in complexation with PLL as a guest molecule, leading to a decreased association number as a result of steric inconsistency. This scheme may also be valid for siRNA complexation, with excess block catiomer inducing a steep drop in association number.

It is interesting that the characteristic mixing ratio where the multimolecular assembly of block catiomer and siRNA occurred shifted to higher N/P with increased IM content. We further investigated this assembly behavior by recalculating N/P ratios in SLI experiments and neglecting the charge contribution from IM groups. (See the Supporting Information.) Multimolecular assembly of PEG-*b*-(PLL-$IM_{0-69\%}$) and siRNA was achieved at 1.2 to 1.5 by the ratio of [unmodified Lys primary amine]/[siRNA phosphate]. It is reasonable to assume that the relatively long-range Coulomb interaction between oppositely charged primary amines and phosphates is the dominant driving force that contributes to multimolecular assembly. However, the monodispersity of multimolecular assemblies was clearly improved with the increased degree of IM substitution (Figure 3a), which might be explained by the chemistry of the amidine bonds of IM groups. Phosphates and amidine analogs such as the guanidino bond in IM groups form relatively strong hydrogen bonds in addition to ionic interactions.[28] This interaction is crucial for strong association of guanidinium groups with phosphates because it was recently shown that methylation of arginine groups and elimination of hydrogen-bonding capability greatly reduced the activity and insertion ability of a short arginine-rich membrane-active peptide toward a phospholipid membrane.[29] It should be noted that hydrogen bond formation requires close contact of proton donors and acceptors, and its contribution can be dramatically reduced in a solvent with a high dielectric constant, such as water.[30] Multimolecular assembly would allow close contact of polymer chains, with the core being rather hydrophobic compared with the exterior medium, and would therefore be favorable for hydrogen bond formation. Thus, initial multimolecular assembly may be driven by long-range electrostatic interaction of primary amines and siRNA phosphates with amidine−phosphate short-range interactions, resulting in a more ordered and uniform micelle core structure. Amidine functional groups might have facilitated unimodal multimolecular assembly of PEG-*b*-(PLL-IM) and

Scheme 1. Preparation of Iminothiolane-Modified Poly(ethylene glycol)-*block*-poly(L-lysine) [PEG-*b*-(PLL-IM)]

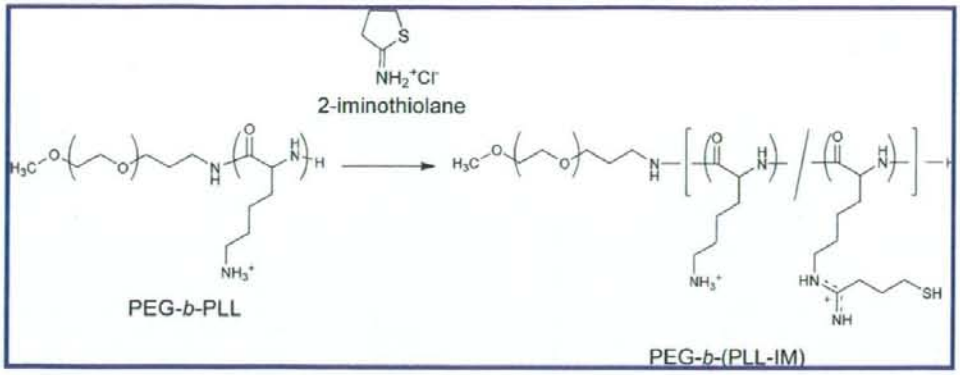

siRNA through intrinsic interaction modes, which are distinct from that of primary amines in unmodified lysines. Additionally, the presence of sulfur-containing side chains in the block copolymer may have also affected the formation of monomodal multimolecular assemblies because of increased hydrophobicity or restriction of the possible orientations to accommodate bulky groups in the micelle core. Interestingly, PIC-Ms formed between PEG-*b*-PLL modified with the sulfur-containing cross-linker N-succinimidyl 3-(2-pyridyldithio)-propionate (SPDP) and siRNA also showed a decrease in size and dispersity with increased thiol modification degree. (See the Supporting Information.) The detailed mechanism of monomodal micelle formation between block copolymer cations and siRNA remains elusive and requires more work to elucidate the interesting assembly behavior observed in this work.

The most important achievement of this work was the identification of the factors required to form unimodal multimolecular assemblies between IM-modified cationic block copolymers and siRNA, yielding siRNA-incorporated disulfide cross-linked PIC-Ms that accomplished highly efficient siRNA transfection. Amidine groups of PEG-*b*-(PLL-IM) were strongly suggested to facilitate unimodal micellar assembly with siRNA, as discussed above, whereas thiols were shown to confer environment responsiveness to resulting PIC micelles through the formation of disulfide cross-links within their cores (Figure 5a). Another important finding was the strong correlation between transfection efficiency and the formation of micellar structure. Even in the disulfide cross-linked system, efficient transfection was achieved only at the critical N/P for micelle formation, a slight deviation from the optimal N/P resulted in a sharp drop in transfection efficacy (compare Figures 2, 3b, and 7c). Resistance of siRNA to enzymatic degradation is not the major reason for this unique property of PIC-Ms because nonmicellar complexes of PEG-*b*-PLL and siRNA formed at N/P = 2 showed appreciable stabilization of siRNA in 70% FBS medium even after 24 h of incubation. (See the Supporting Information.) Apparently, as seen in Figure 8, the incorporation of siRNA in cross-linked PIC-Ms significantly improved cellular uptake, leading to a remarkable gene silencing effect for the micelle composition with optimal cross-linking density.

Conclusions

In this study, we established a method for preparing disulfide cross-linked PIC-Ms from PEG-*b*-(PLL-IM) and siRNA. The formation of PIC-Ms was strictly controlled by the mixing ratio of the block copolymer with siRNA, yielding monodisperse PIC-Ms at only specific N/P ratios. Disulfide cross-linking contributed to the stabilization of otherwise fragile PIC-Ms under physiological salt conditions. Careful tuning of IM modification imparted environmental responsivity of PIC-Ms to reductive conditions, allowing the prompt release of encapsulated siRNA. Effective silencing of the target gene was demonstrated in cultured cells by siRNA-incorporated PIC-Ms with controlled cross-linking density. These results show the promise of PIC-Ms as a building block for the development of highly effective siRNA delivery systems.

Acknowledgment. This study was supported by Special Coordination Funds for Promoting Science and Technology (SCF) commissioned by the Ministry of Education, Culture, Sports, Science, and Technology (MEXT) of Japan.

Supporting Information Available. A summary of size and PDI of PIC-Ms formed with PEG-*b*-(PLL-IM) of various IM compositions and siRNA, residual thiol content of cross-linked PIC-Ms formed with PEG-*b*-(PLL-IM)s and siRNA, size and PDI of PEG-*b*-PLL(IM) PIC-Ms prepared at each optimal N/P at various NaCl concentrations, PIC-$M_{14\%}$ stability versus time, Lipofectamine2000 siRNA transfection efficacy, PIC-$M_{14\%}$ and PEG-*b*-PLL/siRNA PIC cytotoxicity, Cy5 fluorescence quenching after incorporation into PIC-$M_{14\%}$, SLI measurements plotted as a function of the N/P ratio of unmodified primary amines, PEG-*b*-PLL(PDP) structure and corresponding PIC-M properties, and stability of siRNA incorporated PEG-*b*-(PLL-IM) PIC-Ms toward enzymatic degradation are available. This material is available free of charge via the Internet at http://pubs.acs.org.

References and Notes

(1) Elbashir, S. M.; Harborth, J.; Lendeckel, W.; Yalcin, A.; Weber, K.; Tuschl, T. *Nature* **2001**, *411*, 494–498.
(2) Fire, A.; Xu, S. Q.; Montgomery, M. K.; Kostas, S. A.; Driver, S. E.; Mello, C. C. *Nature* **1998**, *391*, 806–811.
(3) Behlke, M. A. *Mol. Ther.* **2006**, *13*, 644–670.
(4) de Fougerolles, A.; Vornlocher, H.-P.; Maraganore, J.; Lieberman, J. *Nat. Rev. Drug Discovery* **2007**, *6*, 443–453.
(5) Morrissey, D. V.; Lockridge, J. A.; Shaw, L.; Blanchard, K.; Jensen, K.; Breen, W.; Hartsough, K.; Machemer, L.; Radka, S.; Jadhav, V.; Vaish, N.; Zinnen, S.; Vargeese, C.; Bowman, K.; Shaffer, C. S.; Jeffs, L. B.; Judge, A.; MacLachlan, I.; Polisky, B. *Nat. Biotechnol.* **2005**, *23*, 1002–1007.
(6) Soutschek, J.; Akinc, A.; Bramlage, B.; Charisse, K.; Constien, R.; Donoghue, M.; Elbashir, S.; Geick, A.; Hadwiger, P.; Harborth, J.; John, M.; Kesavan, V.; Lavine, G.; Pandey, R. K.; Racie, T.; Rajeev, K. G.; Rohl, I.; Toudjarska, I.; Wang, G.; Wuschko, S.; Bumcrot, D.;

Koteliansky, V.; Limmer, S.; Manoharan, M.; Vornlocher, H. P. *Nature* **2004**, *432*, 173–178.
(7) Boussif, O.; Lezoualch, F.; Zanta, M. A.; Mergny, M. D.; Scherman, D.; Demeneix, B.; Behr, J. P. *Proc. Natl. Acad. Sci. U.S.A.* **1995**, 92, 7297–7301.
(8) Goula, D.; Becker, N.; Lemkine, G. F.; Normandie, P.; Rodrigues, J.; Mantero, S.; Levi, G.; Demeneix, B. A. *Gene Ther.* **2000**, *7*, 499–504.
(9) Ge, Q.; Filip, L.; Bai, A. L.; Nguyen, T.; Eisen, H. N.; Chen, J. *Proc. Natl. Acad. Sci. U.S.A.* **2004**, *101*, 8676–8681.
(10) Schiffelers, R. M.; Ansari, A.; Xu, J.; Zhou, Q.; Tang, Q. Q.; Storm, G.; Molema, G.; Lu, P. Y.; Scaria, P. V.; Woodle, M. C. *Nucleic Acids Res.* **2004**, *32*, e149.
(11) de Wolf, H. K.; Snel, C. J.; Verbaan, F. J.; Schiffelers, R. M.; Hennink, W. E.; Storm, G. *Int. J. Pharm.* **2007**, *331*, 167–175.
(12) Kataoka, K.; Togawa, H.; Harada, A.; Yasugi, K.; Matsumoto, T.; Katayose, S. *Macromolecules* **1996**, *29*, 8556–8557.
(13) Katayose, S.; Kataoka, K. *Bioconjugate Chem.* **1997**, *8*, 702–707.
(14) Harada-Shiba, M.; Yamauchi, K.; Harada, A.; Takamisawa, I.; Shimokado, K.; Kataoka, K. *Gene Ther.* **2002**, *9*, 407–414.
(15) Akagi, D.; Oba, M.; Koyama, H.; Nishiyama, N.; Fukushima, S.; Miyata, T.; Nagawa, H.; Kataoka, K. *Gene Ther.* **2007**, *14*, 1029–1038.
(16) Itaka, K.; Kanayama, N.; Nishiyama, N.; Jang, W. D.; Yamasaki, Y.; Nakamura, K.; Kawaguchi, H.; Kataoka, K. *J. Am. Chem. Soc.* **2004**, *126*, 13612–13613.
(17) DeRouchey, J.; Schmidt, C.; Walker, G. F.; Koch, C.; Plank, C.; Wagner, E.; Radler, J. O. *Biomacromolecules* **2008**, *9*, 724–732.
(18) Kakizawa, Y.; Harada, A.; Kataoka, K. *J. Am. Chem. Soc.* **1999**, *121*, 11247–11248.
(19) Kakizawa, Y.; Harada, A.; Kataoka, K. *Biomacromolecules* **2001**, *2*, 491–497.
(20) Miyata, K.; Kakizawa, Y.; Nishiyama, N.; Harada, A.; Yamasaki, Y.; Koyama, H.; Kataoka, K. *J. Am. Chem. Soc.* **2004**, *126*, 2355–2361.
(21) Miyata, K.; Kakizawa, Y.; Nishiyama, N.; Yamasaki, Y.; Watanabe, T.; Kohara, M.; Kataoka, K. *J. Controlled Release* **2005**, *109*, 15–23.
(22) Meister, A.; Anderson, M. E. *Annu. Rev. Biochem.* **1983**, *52*, 711–760.
(23) Harada, A.; Kataoka, K. *Macromolecules* **1995**, *28*, 5294–5299.
(24) Riddles, P. W.; Blakeley, R. L.; Zerner, B. *Anal. Biochem.* **1979**, *94*, 75–81.
(25) Jue, R.; Lambert, J. M.; Pierce, L. R.; Traut, R. *Biochemistry* **1978**, *17*, 5399–5406.
(26) Harada, A.; Cammas, S.; Kataoka, K. *Macromolecules* **1996**, *29*, 6183–6188.
(27) Harada, A.; Kataoka, K. *Soft Matter* **2008**, *4*, 162–167.
(28) Mascotti, D. P.; Lohman, T. M. *Biochemistry* **1997**, *36*, 7272–7279.
(29) Tang, M.; Waring, A. J.; Lehrer, R. I.; Hong, M. *Angew. Chem., Int. Ed.* **2008**, *47*, 3202–3205.
(30) Williams, D. H.; Westwell, M. S. *Chem. Soc. Rev.* **1998**, *27*, 57–63.

BM800985E

Journal of Controlled Release 133 (2009) 245–251

Contents lists available at ScienceDirect

Journal of Controlled Release

journal homepage: www.elsevier.com/locate/jconrel

NANOMEDICINE

Enhanced photodynamic cancer treatment by supramolecular nanocarriers charged with dendrimer phthalocyanine

Nobuhiro Nishiyama [a,1], Yoshinori Nakagishi [d,e,1], Yuji Morimoto [f,*], Ping-Shan Lai [g], Kozo Miyazaki [a,f], Kyoko Urano [a,f], Souta Horie [a], Michiaki Kumagai [a], Shigeto Fukushima [a], Yu Cheng [b], Woo-Dong Jang [h], Makoto Kikuchi [d], Kazunori Kataoka [a,b,c,*]

[a] Center for Disease Biology and Integrative Medicine, Graduate School of Medicine, The University of Tokyo, Tokyo, Japan
[b] Department of Materials Engineering, Graduate School of Engineering, The University of Tokyo, Tokyo, Japan
[c] Center for Nano-Bio Integration, The University of Tokyo, Tokyo, Japan
[d] Department of Medical Engineering, National Defense Medical College, Saitama, Japan
[e] Department of Surgery II, National Defense Medical College, Saitama, Japan
[f] Department of Integrative Physiology and Bio-Nano Medicine, National Defense Medical College, Saitama, Japan
[g] Department of Chemistry, Center of Nanoscience and Nanotechnology, National Chung-Hsing University, Taiwan
[h] Department of Chemistry, College of Science, Yonsei University, Seoul, Republic of Korea

ARTICLE INFO

Article history:
Received 1 August 2008
Accepted 6 October 2008
Available online 26 October 2008

Keywords:
Photodynamic therapy
Phthalocyanine
Dendrimer
Polymeric micelle

ABSTRACT

Photodynamic therapy (PDT) is a promising method for the localized treatment of solid tumors. In order to enhance the efficacy of PDT, we have recently developed a novel class of photosensitizer formulation, i.e., the dendrimer phthalocyanine (DPc)-encapsulated polymeric micelle (DPc/m). The DPc/m induced efficient and unprecedentedly rapid cell death accompanied by characteristic morphological changes such as blebbing of cell membranes, when the cells were photoirradiated using a low power halogen lamp or a high power diode laser. The fluorescent microscopic observation using organelle-specific dyes demonstrated that DPc/m might accumulate in the endo-/lysosomes; however, upon photoirradiation, DPc/m might be promptly released into the cytoplasm and photodamage the mitochondria, which may account for the enhanced photocytotoxicity of DPc/m. This study also demonstrated that DPc/m showed significantly higher *in vivo* PDT efficacy than clinically used Photofrin® (polyhematoporphyrin esters, PHE) in mice bearing human lung adenocarcinoma A549 cells. Furthermore, the DPc/m-treated mice did not show skin phototoxiciy, which was apparently observed for the PHE-treated mice, under the tested conditions. These results strongly suggest the usefulness of DPc/m in clinical PDT.

1. Introduction

Photodynamic therapy (PDT), an effective modality for treating localized tumors, involves the systemic administration of porphyrin- or phthalocyanine-based photosensitizers (PSs), followed by local photoirradiation of solid tumors with the light of a specific wavelength [1–3]. Upon photoirradiation, PSs generate reactive oxygen species (ROS) such as singlet oxygen, leading to photochemical destruction of tumor vessels and tumor tissues. PDT shows a high clinical complete response to early-stage superficial tumors, including lung, esophageal, gastric, and cervical cancers. Also, PDT is quite useful as an initial treatment for malignant tumors because organ functions are maintained, thus saving the patient's stamina for further treatments. However, PDT is known to be accompanied by skin hyperphotosensitivity, so that the patient needs to stay in a darkened room for at least 2 weeks. This effect is attributable to the lack of tumor selectivity by currently approved PSs, such as Photofrin® [3]. Tumor-selective PSs and their formulations are expected to restrain unfavorable side effects and improve the efficacy of PDT against intractable tumors. In this context, the use of long-circulating nanocarriers such as liposomes [4], water-soluble polymers [5–7] and polymeric micelles [8–10] is a promising way to improve the tumor selectivity of PSs. It has been demonstrated that such nanocarriers can preferentially and effectively accumulate in solid tumors, since the tumor tissues are characterized by the enhanced permeability and retention (EPR) effect, which consists of microvascular hyperpermeability to circulating macromolecules and impaired lymphatic drainage [11].

* Corresponding authors. Morimoto is to be contacted at the Department of Integrative Physiology and Bio-Nano Medicine, National Defense Medical College, Namiki 3-2, Tokorozawa, Saitama 359-8513, Japan. Tel.: +81 4 2995 1482; fax: +81 4 2996 5187. Kataoka, Department of Materials Engineering, Graduate School of Engineering, The University of Tokyo, 7-3-1 Hongo, Bunkyo-ku, Tokyo 113-8656, Japan. Tel.: +81 3 5841 7138; fax: +81 3 5841 7139.
E-mail addresses: moyan@ndmc.ac.jp (Y. Morimoto), kataoka@bmw.t.u-tokyo.ac.jp (K. Kataoka).
[1] These authors contributed equally to this work.

0168-3659/$ – see front matter © 2008 Elsevier B.V. All rights reserved.
doi:10.1016/j.jconrel.2008.10.010

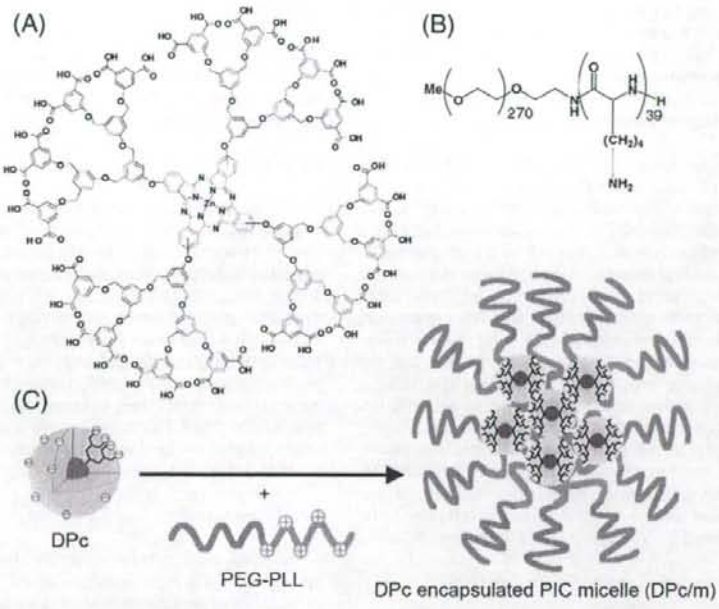

Fig. 1. Chemical structures of anionic dendrimer phthalocyanine (DPc) (A) and poly(ethylene glycol)–poly(L-lysine) (PEG–PLL) block copolymer (B). The DPc-encapsulated polyion complex (PIC) micelle (DPc/m) was formed by mixing DPc and PEG–PLL at a charge stoichiometric ratio (C).

Regarding the development of nanocarriers encapsulating PSs, most conventional PSs may have several serious drawbacks. Since potent PSs generally have large π-conjugation domains, they easily form aggregates due to their π–π and hydrophobic interactions. Such aggregate formation severely decreases the ROS formation essential to the PDT effect [12,13]. Also, this propensity may hamper the encapsulation of PSs into nanocarriers such as liposomes and polymeric micelles. To solve such problems, we have developed ionic dendrimer photosensitizers where the core of porphyrin or phthalocyanine is surrounded by large dendritic wedges [14,15]. Unlike conventional PSs, dendrimer photosensitizers exhibit effective ROS production even at extremely high concentrations, because the dendritic wedges sterically prevent or weaken aggregation of the center dye molecules [13,16]. In addition, ionic groups on the peripheries of dendrimer photosensitizers allow their stable incorporation into polyion complex (PIC) micelles through the electrostatic interaction with oppositely charged poly(ethylene glycol)(PEG)–polyelectrolyte block copolymers [10,13,15,16]. Polymeric micelles, which are characterized by a size of several tens of nanometers and a core–shell architecture, are potent nanocarriers for site-specific drug delivery, as several formulations encapsulating antitumor agents have already progressed to clinical studies [17–19]. We have already demonstrated that PIC micelles encapsulating third-generation dendrimer porphyrin showed remarkably high photocytotoxicity against cancer cells and successfully treated experimental disease models of choroidal neovascularization (CNV) in rats [20], indicating that dendrimer photosensitizer-encapsulated PIC micelles show great promise for use in clinical PDT.

Recently, we prepared PIC micelles through the electrostatic interaction between the anionic dendrimer phthalocyanine (DPc) and the PEG–poly(L-lysine) block copolymer (PEG–PLL) (Fig. 1) [15]. Since DPc has strong Q-band absorption at 685 nm, at which the light deeply penetrates tissues, the DPc-encapsulated PIC micelle (DPc/m) is assumed to be effective in PDT of solid tumors. In our previous paper, DPc/m showed approximately three- to four-fold decrease in the oxygen consumption rate compared with free DPc, indicating a decrease in quantum yield of singlet oxygen formation [15]. Compared with aforementioned dendrimer porphyrin, a relatively small dendritic wedge of DPc may not entirely prevent collisional quenching in the micellar core. Nevertheless, DPc/m displayed approximately 100-fold higher *in vitro* photocytotoxicity against human cervical cancer HeLa cells compared with free DPc when the cells were photoirradiated for 60 min with broad-band light (400–700 nm) using a low power halogen lamp [15]. However, the underlying mechanisms of the enhanced photocytotoxicity of DPc/m remain to be clarified yet, because DPc/m showed only 4 times higher cellular uptake compared with free DPc. In the present paper, we have studied *in vitro* photocytotoxicity of DPc/m when human lung adenocarcinoma A549 cells were photoirradiated by a diode laser (670 nm), and found that DPc/m showed unique photochemical processes inside of the cells to induce cell death in an unprecedentedly fast manner. Also, we have studied *in vivo* antitumor activity of DPc/m against subcutaneous tumor models in mice.

2. Materials and Methods

2.1. Preparation of DPc and DPc/m

The synthesis of anionic dendrimer phthalocyanine (DPc) has been reported previously [15,21]. The synthesized DPc is composed of the 2nd generation aryl ether dendrimer with a Zn(II)-phthalocyanine center and 32 carboxylic groups on its periphery (Fig. 1A). Poly(ethylene glycol)–poly(L-lysine) block copolymer (PEG–PLL) (Fig. 1B) was synthesized by the polymerization of the *N*-carboxy anhydride of N^{ε}-Z-L-lysine initiated by CH_3O-PEG-NH_2 (12,000 g/mol), followed by deprotection of the Z group according to a previously reported method [22]. The polymerization degree of PLL segment was determined to be 39 by the ^1H NMR measurement. The DPc-encapsulated PIC micelle (DPc/m) was prepared at a charge stoichiometric ratio of negatively-charged DPc and positively-charged PEG–

PLL (Fig. 1C). The resulting DPc/m had a diameter of ca. 50 nm with a narrow size distribution (unimodal, $\mu_2/\Gamma^2 = 0.12$) and zeta-potential value of −0.56±0.56 mV, which were measured by a Zetasizer nanoseries (Malvern Instruments Ltd., UK).

2.2. Cell culture and cytotoxicity assay

Human lung adenocarcinoma A549 cells were obtained from Riken Bioresource Center Cell Bank (Tsukuba, Japan). A549 cells were maintained in Dulbecco's modified Eagle medium (Invitrogen, Carlsbad, CA) containing 10% fetal bovine serum in a humidified atmosphere containing 5% CO_2 at 37 °C. The light-induced cytotoxicity (photocytotoxicity) of each photosensitizing agent was evaluated as follows: In a darkened room, the cells were incubated with photosensitizing agents for 24 h. After washing with PBS and medium replacement, the cells were photoirradiated using a low power halogen lamp or a high power diode laser. In the former case, the culture plate was irradiated with broad-band visible light using a halogen lamp equipped with a filter passing light of 400–700 nm (fluence rate: 3.0 mW/cm^2; irradiation time: 15, 30, 45, and 60 min; fluence: 2.7–10.8 J/cm^2). In the latter case, each well was photoirradiated by a 670 nm, continuous wave diode laser (HLD2000MT 7A, High Power Devices, North Brunswick, NJ) (fluence rates: 25, 50, and 100 mW/cm^2; irradiation time: 1000 s; fluence: 25–100 J/cm^2). The cell viability was evaluated by MTT assay 24 h after photoirradiation.

2.3. Observation of morphological changes of the cell during photoirradiation

To investigate the modality of light-induced cell death, we examined the morphological changes occurring in DPc- and DPc/m-treated cells during photoirradiation in a time-lapse manner. In this experiment, A549 cells were incubated with DPc or DPc/m for 24 h at the 99% cell growth-inhibitory concentration (IC_{99}). After the medium was replaced, the morphological changes in the cells during photoirradiation by the light source of a time-lapse sectioning fluorescent microscope (ApoTome/Axiovert 200 M, Carl Zeiss, Oberkochen, Germany; fluence rate: ~120 mW/cm^2) were continuously monitored using the microscope's differential interference contrast (DIC) mode. In addition, the fluorescent images from DPc and Rhodamine 123 (Rh123) (Molecular Probes, Eugene, OR), a specific dye to the mitochondria, were simultaneously observed.

2.4. Intracellular localization of DPc/m

To evaluate the intracellular localization of DPc/m, PEG–PLL was labeled with Alexa fluor 488 carboxylic acid, succinimidyl ester (5.0 mg, 7.8 μmol) (Invitrogen) according to the manufacturer's protocol. After removal of unbound dye by dialysis and lyophilization, the ratio of the dye to PEG–PLL was estimated to be 3.8 by measuring UV–Vis spectra. The Alexa 488-labeled DPc/m was prepared as above-mentioned.

Intracellular localization of Alexa 488-labeled DPc/m in A549 cells was observed by confocal laser scanning microscopy (CLSM) (LSM510META, Carl Zeiss). After 24-h incubation with Alexa 488-labeled DPc/m and subsequent washing, the cells were treated with LysoTracker Red DND-99, MitoTracker Red 580, and ER Tracker Red (Molecular Probes) for the staining of endo-/lysosomes, mitochondria, and endoplasmic reticulum, respectively. The fluorescent images of the cells without photoirradiation were observed by CLSM.

2.5. Measurement of ROS production in the mitochondria

The ROS production in the mitochondria in A549 cells was detected by MitoSOX Red reagent (Invitrogen), which rapidly accumulates in the mitochondria and exhibits fluorescence upon oxidation by superoxide and other ROS. After 24-h incubation with DPc or DPc/m, the cells were incubated with MitoSOX Red (5 μM) for 10 min at 37 °C. Then, the fluorescent image of MitoSOX Red in living cells during photoirradiation using the light source of the microscope was observed by CLSM (TCS SP2 Spectral Confocal System, Leica, Nussloch, Germany).

2.6. In vivo antitumor effect

The antitumor activity of DPc, DPc/m or Photofrin® (porfimer sodium, PHE from Wyeth, Madison, NJ) was tested against subcutaneous tumor models of A549 cells in mice ($n = 6$). A549 cells (3×10^6) were subcutaneously transplanted into the left back of 6-week-old female nude mice (BALB/c *nu/nu*) (Clea Japan, Tokyo, Japan). Fifteen days after transplantation, one of the photosensitizing agents was administered intravenously at a dose of 1.85 mg/kg (0.37 μmol/kg photosensitizing unit) for DPc and DPc/m and 1.65 mg/kg (2.7 μmol/kg photosensitizing unit) for PHE. Twenty-four hours after the administration, tumor sites were irradiated with a diode laser with a light dose of 100 J/cm^2. This animal study protocol was approved by the Ethics Committee for Laboratory Animals of the National Defense Medical College, Tokorozawa, Japan.

2.7. Skin phototoxicity

Six-week-old female nude mice (BALB/c *nu/nu*) were intravenously administered 4.2 μmol/kg DPc/m or 8.1 μmol/kg Photofrin® (PHE), followed by white light irradiation to abdominal skin using a halogen lamp at the fluence of 60 J/cm^2 at 0.5, 1, 2 or 4 days after administration. Four days after irradiation, macroscopic changes in the skin as well as in the organs were observed.

3. Results

3.1. In vitro PDT using halogen lamp

Table 1 summarizes the 50% cell growth inhibitory concentrations (IC_{50}) of DPc, DPc/m and Photofrin® (PHE) against A549 cells. Note that none of the photosensitizing agents showed dark toxicity. As shown in Table 1, DPc/m exhibited an irradiation time-dependent increase in cytotoxicity, which is consistent with our previous results of the photocytotoxicity against HeLa cells [14]. Eventually, DPc/m achieved 78-fold higher photocytotoxicity than free DPc at 10.8 J/cm^2. It is worth mentioning that DPc/m was 3.9 times more effective than even clinically used PHE on a molar basis of photosensitizing units.

3.2. In vitro PDT using diode laser

The photocytotoxicity of DPc and DPc/m against A549 cells are summarized in Table 2 and Fig. S1 in Supporting Information. As shown in Table 2, DPc/m exhibited 44-fold higher photocytotoxicity than DPc at 25 J/cm^2. It is noteworthy that DPc displayed a fluence-rate-dependent increase in photocytotoxicity, whereas DPc/m was

Table 1
In vitro cytotoxicity of photosensitizing agents after photoirradiation using halogen lamp

Photoirradiate condition		IC_{50} (μM)[a] of photosensitizing agent		
Time (min)	Fluence (J/cm^2)	DPc	DPc/m	PHE
0	0	N.D.[b]	N.D.	N.D.
15	2.7	N.D.	1.0	1.0
30	5.4	N.D.	0.20	0.60
45	8.1	N.D.	0.20	0.35
60	10.8	7.0	0.090	0.35

[a] 50% cell growth-inhibitory concentration.
[b] IC_{50} was higher than the highest examined concentration (20 μM).

Table 2
In vitro cytotoxicity of photosensitizing agents after photoirradiation using diode laser

Photoirradiate condition	IC_{50} (μM) of photosensitizing agent	
Fluence (J/cm^2)	DPc	DPc/m
25	20	0.45
50	4.8	0.16
100	0.86	0.11

less influenced by the fluence rate. Eventually, DPc/m showed only 7.9-fold higher photocytotoxicity than DPc at 100 J/cm^2.

3.3. Observation of morphological changes of the cell during photoirradiation

The morphological changes occurring in the DPc- and DPc/m-treated cells during photoirradiation were monitored in a time-lapse manner. The observations revealed marked differences between DPc and DPc/m (Fig. 2). The DPc/m-treated cells swelled rapidly, accompanied by membrane blebbing, resulting in the disappearance of the initial shape of the cells within a few minutes of photoirradiation. In contrast, the DPc-treated cells showed gradual shrinkage while maintaining their pseudopodial structures during photoirradiation.

In addition, the fluorescent images from DPc and Rh123, a specific dye to the mitochondria, were simultaneously monitored and are also shown in Fig. 2. Regarding the fluorescence from DPc (red), the DPc-treated cells exhibited a transient burst in the fluorescence: the fluoresce of DPc increased appreciably 60–180 s after the initiation of photoirradiation and became obscure within 400 s. Such unique behavior was also seen in the DPc/m-treated cells; however, the fluorescent burst occurred faster than DPc. On the other hand, there were characteristic differences in the Rh123 fluorescence (green). The Rh123 fluorescence in the DPc/m-treated cells disappeared immediately after the initiation of light irradiation. In contrast, the fluorescence of Rh123 in the DPc-treated cells remained even after 450 s photoirradiation. These results suggest that DPc/m might affect mitochondrial functions during photoirradiation, leading to rapid cell death with characteristic morphological changes.

3.4. Intracellular localization of DPc/m

The intracellular localization of DPc/m in A549 cells before photoirradiation was observed by CLSM. The fluorescence image in Fig. 3A reveals that Alexa 488-labeled DPc/m showed punctate fluorescence co-localized with LysoTracker Red DND-99. In contrast, the fluorescence pattern of Alexa 488-labeled DPc/m was apparently different from those of MitoTracker Red 580 and ER Tracker Red, as shown in Fig. 3B and C, respectively. We also observed the intracellular localization of DPc and DPc/m after 24-h incubation by utilizing DPc's fluorescence, and found that both of them were co-localized with LysoTracker Green DND-26 (Fig. S2 in Supporting Information). These results indicate that DPc and DPc/m may have been internalized through the endocytic pathway and may have localized in the endo-/lysosomes before photoirradiation.

3.5. Measurement of ROS production in the mitochondria

Since DPc/m is assumed to affect the mitochondria, as suggested in Fig. 2, we evaluated ROS production in the mitochondria of A549 cells using MitoSOX Red. As shown in Fig. 4, MitoSOX Red exhibited apparent fluorescence in the DPc/m-treated cells after 1 min photoirradiation, whereas no appreciable fluorescence appeared in the DPc-treated cells even after prolonged photoirradiation. Thus, DPc/m might induce photodamage to the mitochondria and thus affect their functions.

3.6. In vivo antitumor effect and skin phototoxicity

The mice bearing subcutaneous A549 tumors were treated with the PDT using DPc, DPc/m or Photofrin® (PHE), and the relative tumor volumes after photoirradiation are shown in Fig. 5. As a result, the tumors in the DPc/m-treated mice grew significantly slower than those in the DPc-treated mice. It is worth mentioning that the PDT effect of DPc/m was superior to that of PHE, although the injected dose of DPc/m was 7.3-fold lower than that of PHE on the basis of photosensitizing units. On the other hand, we also evaluated *in vivo* phototoxicity after PDT. As shown in Fig. 6B, severe damage to the skin and liver was observed in PHE-administered mice (8.1 μmol/kg photosensitizing unit). In contrast, DPc/m did not induce such damage, although a relatively high dose of DPc/m (4.2 μmol/kg photosensitizing unit) was administered in this study (Fig. 6A). Thus, DPc/m was demonstrated to be a safe but effective photosensitizer formulation over clinically used PHE.

4. Discussion

The targeted delivery of PSs using nanocarriers such as liposomes and polymeric micelles have been studied to improve the therapeutic efficacy and restrain side effects in PDT [4–10,13–16]. The use of nanocarriers is expected to increase the concentration of PSs in the tumor tissue based on the EPR effect [10]; however, incorporation of

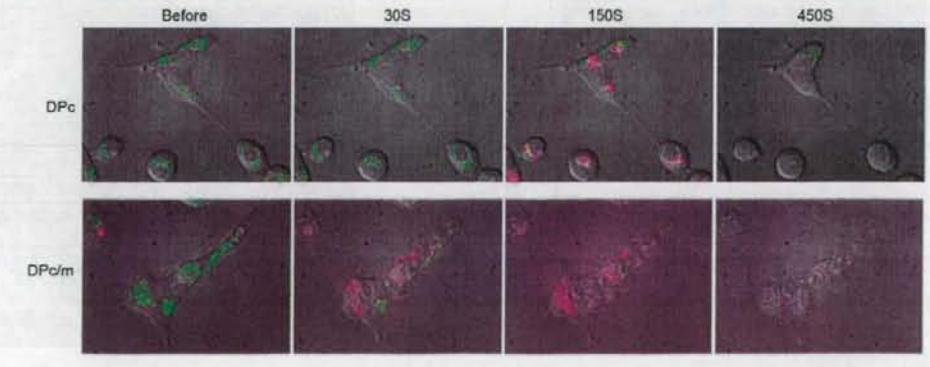

Fig. 2. Time-dependent morphological changes of the DPc- and DPc/m-treated A549 cells during photoirradiation. The fluorescences from DPc (red) and Rhodamine 123 (Rh123) (green) were simultaneously monitored.